Research Square

Preprints are preliminary reports that have not undergone peer review.
They should not be considered conclusive, used to inform clinical practice,
or referenced by the media as validated information.

High-throughput Screening of Stable and Efficient Double Inorganic Halide Perovskite Materials by DFT

Xinfeng Diao (diaoxinfeng77@126.com)
Shangqiu Normal University
Yongxin Diao
Henan Zhongfen Instrument Co., Ltd
Yanlin Tang
Guizhou University
Gangling Zhao
Shangqiu Normal University
Qinzhong Gu
Shangqiu Normal University
Yu Xie
Shangqiu Normal University
Yebai Shi
Shangqiu Normal University
Liang Zhang
Shangqiu Normal University
Ping Zhu
Shangqiu Normal University

Article

Keywords: perovskite, chemical stability, DFT, solar cell

Posted Date: April 25th, 2022

DOI: https://doi.org/10.21203/rs.3.rs-1565189/v1

License: This work is licensed under a Creative Commons Attribution 4.0 International License.
Read Full License

High-throughput Screening of Stable and Efficient Double Inorganic Halide Perovskite Materials by DFT

Xinfeng Diao*[a,b] Yongxin Diao*[c] Yanlin Tang[b] Gangling Zhao[a] Qinzhong Gu[a] Yu Xie[a] Yebai Shi[a] Ping Zhu[a] Liang Zhang[a]

a. College of electronic and electrical engineering, Shangqiu Normal University, Shangqiu 476000 China

b. College of Physics, Guizhou University, Guiyang 550025, China

c. Henan Zhongfen Instrument Co., Ltd. Shangqiu 476000 China

Abstract

In this paper, the photoelectric conversion properties and stability of 42 inorganic double perovskite materials were studied based on density functional theory (DFT). Starting from the construction of double perovskite crystal structures, the data mining algorithm in informatics was introduced into the analysis of high-throughput computing data. The results show that the tolerance factors of 39 crystals are between 0.8 and 1.10, indicating that these crystals have a stable perovskite structure. Then, the important parameters such as dielectric function, PDOS, elastic modulus, shear modulus and Poisson's ratio of the crystal were analyzed. Considering the band gap structure and absorption spectrum, it is found that the light absorption curves of Cs_2SeI_6, Cs_2SeBr_6 Rb_2SeI_6, Rb_2SeBr_6, and Rb_2SeCl_6 fall in a relatively large range in the visible light region. Further considering the stability factor Cs_2SeI_6, Rb_2SeI_6, Cs_2SeBr_6 and Rb_2SeBr_6 can be considered as ideal candidates for light absorbing materials, providing a basis for the industrial application of solar cells.

Key words: perovskite, chemical stability, DFT , solar cell

PACS: 78.56.-a 81.05.Fb 42.50.Nn

1 Introduction

Perovskite materials are widely used in solar cells due to their tunable band gap, strong light absorption, long carrier diffusion length, and small exciton binding energy [1-12]. Since the first application in 2009 for perovskite materials, it has developed rapidly in just a few years. The photoelectric conversion efficiency (PCE) of metal halide perovskite-configured solar cells rises from 3.8% for dye-sensitized solar cell configurations to 25.7% for planar heterojunction cells

which was certified by National Renewable Energy Laboratory (NREL) [13-22]. Organic/inorganic perovskite ($CH_3NH_3PbI_3$, $NH_2CH{=}NH_2PbI_3$) solar cells have reached commercially viable efficiency levels. The current obstacle to commercialization is the stability of perovskite solar cells. The specific solution is to improve humidity stability, allowing the module to operate in an outdoor environment without expensive packaging methods, and no environmental pollution is found. Metal halides replace harmful elements such as lead (Pd) [23]. There have been many recent reports on perovskites ($CH_3NH_3PbX_3$) are stable for hundreds of hours when exposed to air in the dark [24, 25], but their stability will decrease when expose to both humidity and sunlight [26]. Fortunately, the situation improves if we expand our search from ternary $A^+B^{2+}X_3$ perovskites to quaternary $A^+{}_2B^{4+}X_6$ double perovskites. The combined advantages of the halide double perovskite Cs_2TiX_6 with low cost, high efficiency, nontoxicity, stability, and tunable bandgap have also been recently reported [27-32]. On the other hand, many studies have shown that replacing MA^+ or FA^+ with cesium cation (Cs^+) (Rb^+) can significantly improve their thermal stability has been reported [6]. These perovskite materials are considered suitable as carrier transport materials (CTM) for $CsPbBr_3$ and Cs_2TiBr_6 in light-collecting or light-emitting devices. Double inorganic halide perovskites are direct bandgap semiconductors with strong visible light absorption [33]. And there are many +4 ions in nature, such as Ge^{4+}, Zr^{4+}, Sn^{4+}, Hf^{4+}, Se^{4+}, Te^{4+}, and Pd^{4+} which can be combined with monovalent metal ions Cs^+, Rb^+, they form the double perovskite structure and have suitable electronic configuration, when exposed to very stable in air.

So far, there is no report about systematically study on the optoelectronic properties and stability of double perovskite halide materials by the method of high-throughput screening. In this paper, the properties of inorganic metal halide perovskite materials are comprehensively discussed based on density functional theory (DFT). Factors of band gap structure (conduction band, valence band position) electronic density of states, absorption spectrum and elastic constant, etc., provide a batch of possible high-quality crystal models for experimental exploration of new perovskite solar cells.

2 Computational methods

The calculations in this paper are mainly performed by the plane wave pseudopotentials method as implemented in Cambridge serial total energy package (CASTEP) in Material Studio,

and some parameter verification calculations are carried out by using DMOL^3 Code [33-36]. The calculation of the Dmol^3 software package adopts the numerical basis set, which has high calculation efficiency and is convenient to analyze the minimum value of the bottom of the conduction band and the maximum value of the top of the valence band, and can also calculate aperiodic crystals; while the calculation of castep uses plane waves basis set. In theory, the calculation result of castep is more accurate. The generalized gradient approximation (GGA) within the Perdew–Burke–Ernzerhof (PBE) functional was used for the evaluation of exchange–correlation interactions for two computational modules. The electronic configurations $5s^1$, $5s^25p^2$, $3s^23p^5$, $4s^24p^5$ and $5s^2\,5p^5$ were considered in valence for Rb, Sn, Cl, Br and I atoms, respectively. and the cut-off energy is also set to 500 eV. The structure optimization process stops until the atomic Hellmann-Feynman force is less than 0.01 eV/Å, and the energy convergence criterion is set to 10^{-5} eV. The above parameters have been tested, and the increase has no significant effect on the results. The conduction band and valence band edge positions are calculated with the DMOL3 module [37,38].

3 Model for perovskite solar cells

In this section, we consider inorganic halide double perovskite A_2BX_6 and its crystal structure (shown in Fig. 1), where A is a monovalent cation, B is a tetravalent cation, and X is a halide anion) type perovskite. For perovskite compounds, the octahedral factor is used to predict the formation of BX_6 octahedra, and the tolerance factor is used to predict calcium Formation and distortion of the titanite structure empirically. Likewise, in the perovskite crystal-derived structure A_2BX_6, we can combine the octahedral factor and the radius ratio to predict the formation and deformation of the structure, where A = Cs, Rb, B = Ge, Zr, Sn, Hf, Se, Te and Pd, and the halide anions X = I, Cl, Br. High-throughput screening methods and properties of important elements was shown in Fig 2. The small octahedral factor indicates that it is not favorable for the formation of BX6 octahedra. Small radius ratios lead to evacuated cavities and lower structural symmetry, even different connectivity of fully octahedral networks. Each crystal structure parameter of these compounds was obtained from the International Crystal Structures of Database (ICSD) synthesized and characterized by experiments [39，40]

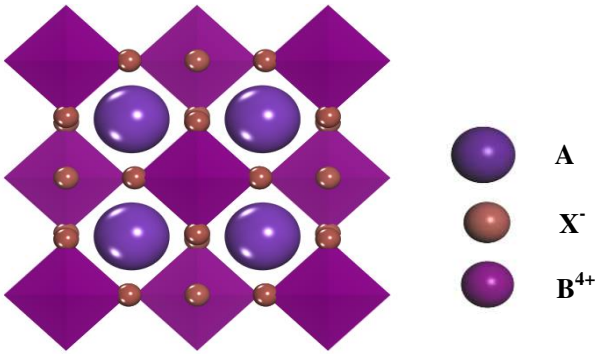

Fig. 1 The crystal structure model of A_2BX_6

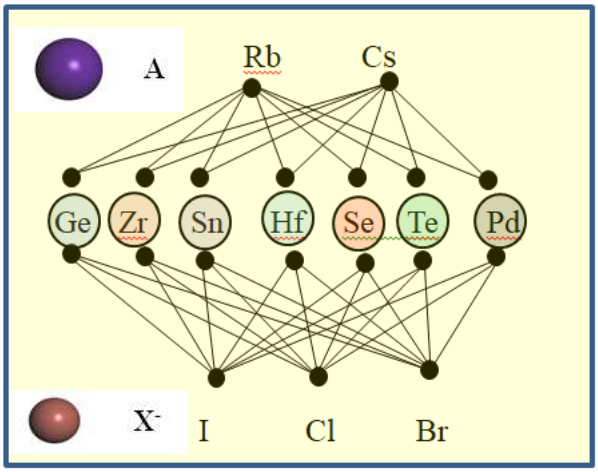

B4+		32 Ge 锗 53 pm	34 Se 硒 50 pm
40 Zr 锆 72 pm	46 Pd 钯 61.9 pm	50 Sn 锡 69 pm	52 Te 碲 97 pm
72 Hf 铪 71 pm			
ⅣB	Ⅷ	ⅣA	ⅥA

Fig. 2 High-throughput screening methods and properties of important elements

To evaluate the structural stability of materials in perovskite structures, we further explore the empirical tolerance factor, which is an important parameter for evaluating whether cations in perovskite materials can be substituted. This factor has been widely used by previous researchers [41] in the current double perovskite A_2BX_6, and the effective [42,43] tolerance factor t can be defined as

$$t = \frac{R_A + R_X}{\sqrt{2}\left[R_B + R_X\right]} \quad (1)$$

In the formula, if there are multiple ions in A and B position, the average radius can be taken. It is a semi-empirical formula that can roughly describe the stability of the perovskite structure. Studies have shown that the tolerance factor of structurally stable perovskite compounds is generally between 0.78 and 1.10. In general：(1) When tolerance factor t is close to 1.0, the compound has an equiaxed Pm3m structure. (2) If tolerance factor t deviates greatly from 1.0, other structures will be formed, in which R_{Cs}=167 pm, R_{Rb}=152 pm, R_I=220 pm, R_{Cl}=181 pm, R_{Br}=196 pm. The calculation result of tolerance factor t is shown in Figure 3.

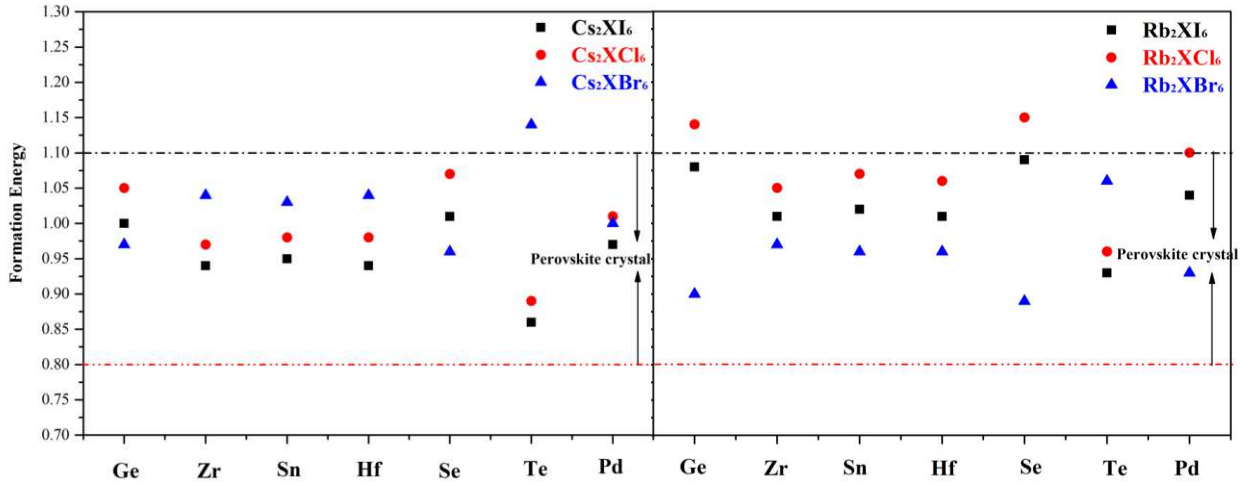

Fig. 3 Tolerance factor of A_2BX_6

The results show that only three tolerance factors of Rb_2GeI_6, Rb_2SeI_6, Cs_2TeI_6 are (1.14, 1.15, 1.14) slightly larger than 1.10, and the tolerance factors of other crystals are all between 0.8-1.10. The result shows that these combinations are in line with the properties of perovskite compound materials. Next, the lattice parameters of these crystals were analyzed, and all possible combinations of crystal compounds were constructed based on the structure of the crystals using MS software, and the crystal parameters were optimized which was shown in figure 4.

	Ge	Zr	Sn	Hf	Se	Te	Pd

Cs(X=I)	a=b=c= 12.08	a=b=c= 12.09	a=b=c= 12.66	a=b=c= 12.00	a=b=c= 12.09	a=b=c= 12.66	a=b=c= 11.76
Rb(X=I)	a=b=c= 12.08	a=b=c= 12.09	a=b=c= 11.85	a=b=c= 12.09	a=b=c= 12.09	a=b=c= 8.25	a=8.33 b=12.66 c=14.68
Cs(X=Cl)	a=b=c= 10.57	a=b=c= 10.79	a=b=c= 10.67	a=b=c= 10.70	a=b=c= 10.67	a=b=c= 10.85	a=b=c= 10.53
Rb(X=Cl)	a=b=c= 10.57	a=b=c= 10.45	a=b=c= 10.41	a=b=c= 10.70	a=b=c= 10.33	a=b=c= 10.52	a=b=c= 10.18
Cs(X=Br)	a=b=c= 11.24	a=b=c= 11.24	a=b=c= 11.24	a=b=c= 11.14	a=b=c= 11.26	a=b=c= 11.26	a=b=c= 10.99
Rb(X=Br)	a=b=c= 11.00	a=b=c= 11.00	a=b=c= 11.00	a=b=c= 11.14	a=7.83 b=7.83 c=11.23	a=b=c= 7.83	a=b=c= 10.72

Fig. 4 Lattice parameters of A_2BX_6

The value of the band gap of the crystal material is an important factor affecting the light absorption efficiency of the perovskite layer. It is well known that the smooth transition of electrons from the valence band to the conduction band can be achieved only when the photon energy $h\nu$ is greater than the band gap of the crystal. In order to analyze the optical properties of these materials, we calculate the band gaps of 42 kinds of materials with CASTEP and DMOL[3] modules, as shown in Figure 5. Refer to the calculation results of some general perovskite materials in other papers ref. Table I, our calculated band gap results are agree with them very well.

Table I Some known band gap reference values of perovskite crystals

Name	This result	Reference	Name	This result	Reference
Cs_2SeCl_6	2.99	2.95 eV[44]	Cs_2HfBr_6	3.30	3.3 eV[46]
Cs_2TeCl_6	3.07	3.10 eV[44]	Cs_2HfI_6	2.23	2.18 eV[46]
Cs_2SeBr_6	1.68	2.64eV [45]	Cs_2HfCl_6	4.226	4.12 eV[46]
Cs_2SeI_6	1.394	1.15eV [45]	Cs_2ZrI_6	1.856	1.92 eV[47]

It can be seen from Figure 5 that the value of band gap for 14 kinds of crystals are between 1.33 and 2.45 eV, such as Cs_2ZrI_6, Cs_2HfI_6, Cs_2SeI_6, Cs_2TeI_6, Rb_2ZrI_6, Rb_2HfI_6, Rb_2SeI6, Rb_2TeI6,

Cs_2GeCl_6, Rb_2GeCl_6, Cs_2SnBr_6,Cs_2SeBr_6 , Rb_2HfBr_6, Rb_2SeBr_6, they are more suitable as light-absorbing layer materials. And the band gap size of the iodine-containing halide perovskite material shows relatively excellent visible light absorption performance, and its performance is better than that of the perovskite material containing Br and Cl halide.

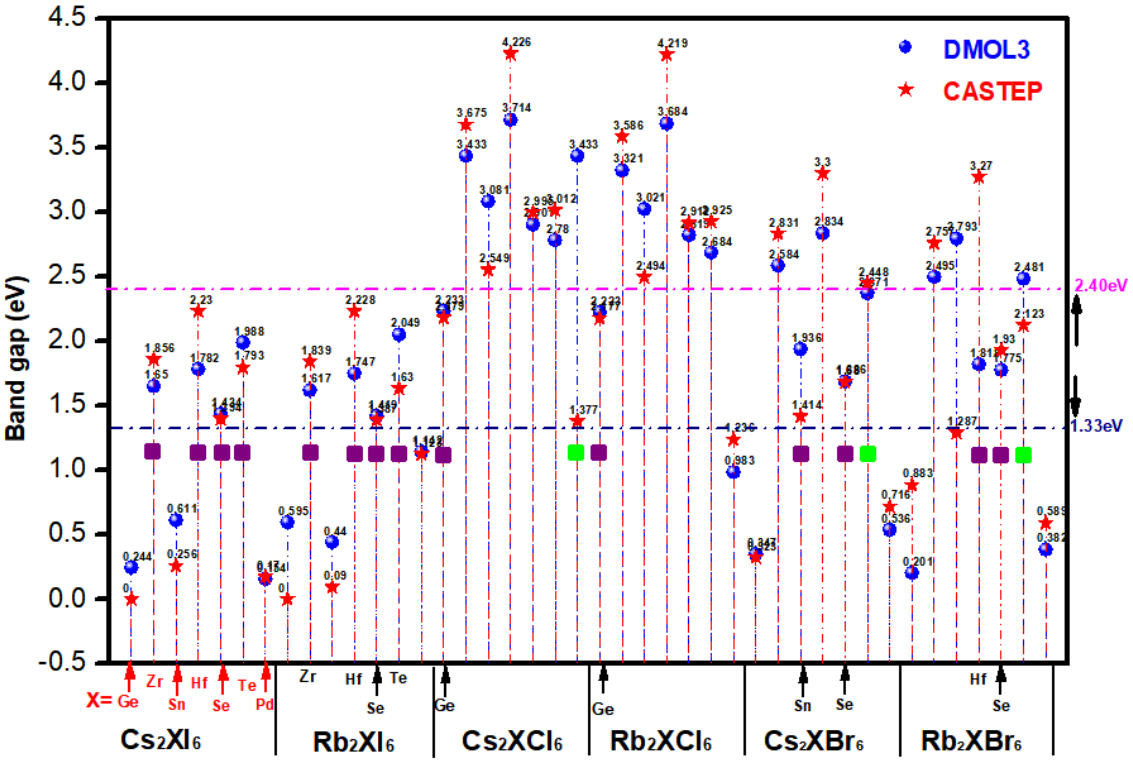

Fig. 5 The value of bandgaps for A_2BX_6

4 Electronic properties of A_2BX_6

As a photoelectric conversion material for solar cells, the electronic structure of A_2BX_6 is a key factor affecting spectral absorption. Therefore, we further analyzed the energy band structures of these materials, and we compared the electric potential of the back electrode of the hole transport layer in the conducting glass in perovskite solar cells. Figure 6 shows that the conduction band position of the perovskite is higher than the conduction band potential value of the electron transport layer, and the valence band position is lower than the potential value of the hole transport layer, which is more conducive to the separation of electrons and holes and forms a stable potential difference external power supply.

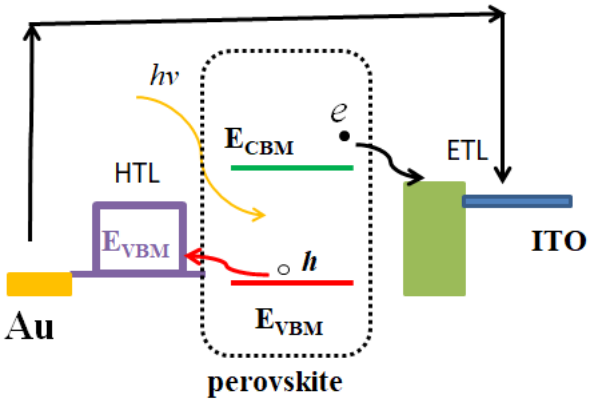

Fig. 6 The device configuration and working principle of perovskite solar cells

The perovskite light-absorbing layer absorbs solar photons to achieve electron-hole separation. The position of the valence band is lower than that of the hole transport material, and the minimum value of the conduction band is higher than that of the electron transport material. The position of the conduction band can realize the smooth separation of carriers.

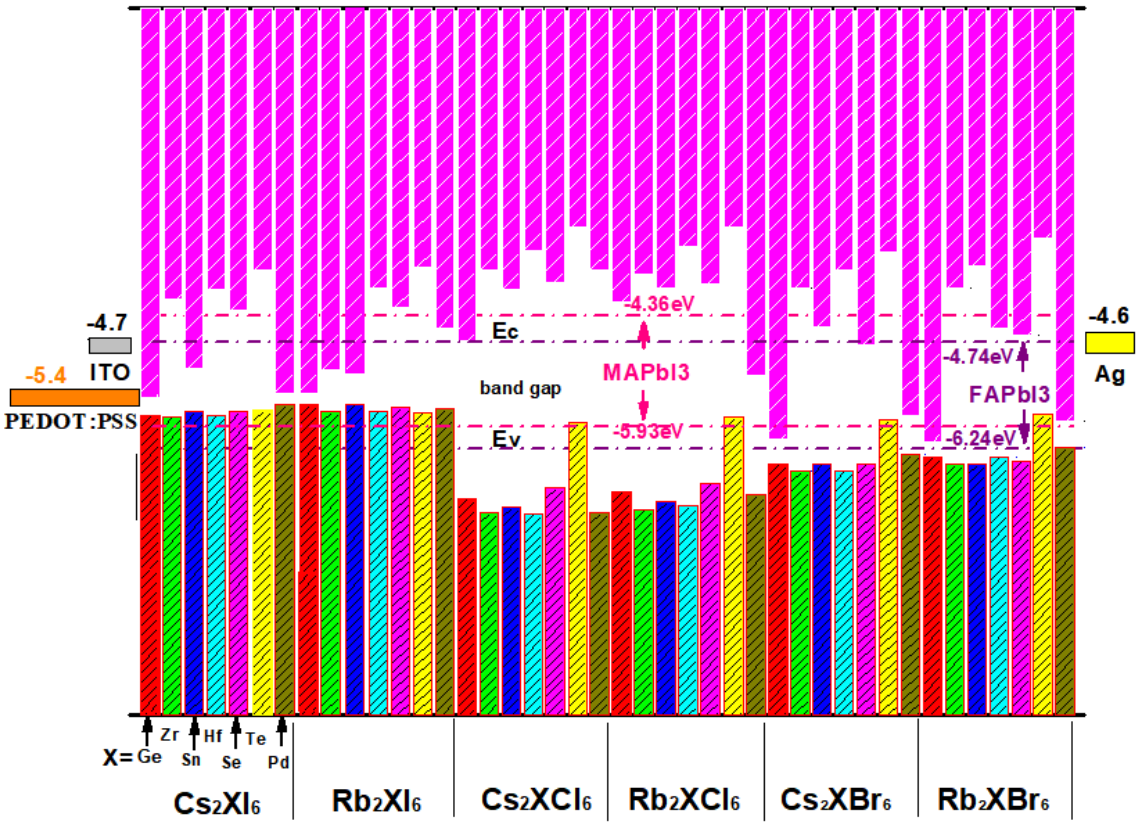

Fig. 7 The valence band maxima (VBM) and conduction band minima (CBM) of 42 crystals

We calculated the valence band maxima (VBM) and conduction band minima (CBM) of 42 compounds and compared them with the band gaps of two efficient organic/inorganic perovskite materials ($CH_3NH_3PbI_3$, $NH_2CH{=}NH_2PbI_3$) from. It can be seen from Fig. 7 that the maximum value of the valence band of these materials and the size of the valence band of the electron transport layer material, the hole transport layer and the back electrode material are helpful to analyze the efficiency of carrier migration of these materials. Priority is given to the above-mentioned 14 materials whose band gaps are between 1.33 and 2.40, the minimum edge of the conduction band is greater than -4.6eV, and the maximum value of the valence band is lower than 5.4eV such as Cs_2ZrI_6, Cs_2HfI_6, Cs_2SeI_6, Cs_2TeI_6, Rb_2HfI_6, Rb_2SeI_6, Rb_2TeI_6, Rb_2GeCl_6 and Rb_2HfBr_6 with larger band gaps may be used in the ultraviolet region.

4.1 Optical properties

The dielectric function ε(ω) is used to describe the linear response characteristics of photovoltaic materials to electromagnetic radiation, and is one of the effective indicators to reflect the spectral characteristics of photovoltaic materials. Its optical response characteristics can be described by the following complex dielectric function ε(ω) [48]

$$\varepsilon(\omega) = \varepsilon_1(\omega) + i\varepsilon_2(\omega) \tag{2}$$

Where $\varepsilon_1(\omega) = n^2 - k^2$, $\varepsilon_2(\omega) = 2nk$ （n and k are the reflection coefficient and extinction coefficient, respectively）ε_1 (ω) andε_2(ω) are the real and imaginary parts of the dielectric function, respectively, depending on the optical frequency. The characteristic curve of the real part of the dielectric function obtained by calculation is shown in Figure 8, and the characteristic curve of the imaginary part is shown in Figure 9. ω represents the frequency of light.

The absorption coefficient is directly related to the band gap of the material. Optical properties can be obtained from complex dielectric functions. The absorption coefficient I(ω) can be derived from $\varepsilon_1(\omega)$ and $\varepsilon_2(\omega)$. The specific formula of the equation is as follows [48]:

$$I(\omega) = \sqrt{2}\omega\left[\sqrt{\varepsilon_1(\omega) + \varepsilon_2(\omega)} - \varepsilon_1(\omega)\right]^{1/2} \tag{3}$$

Next, the optical absorption coefficients of these 42 compounds were calculated by the PBE method and are shown in Fig. 10. Absorption is seen at energies less than the bandgap, which is due to an error in the calculation method and does not affect our analysis of the results. The

absorption coefficient is as high as 10^5 cm^{-1}, which is mainly due to the absorption between the p orbitals of halide ions Cl, Br, and I in the valence band and the s orbital of Sn in the conduction band. Shown in Figure 10 is the absorption spectrum. The optical absorption coefficients of the three structures are shown in Fig. 10. When X changes from I^- to Cl^-, the absorption spectrum of Cs_2TeX_6 is blue-shifted due to the band gap increase. Comparatively, A_2XI_6 has better absorption

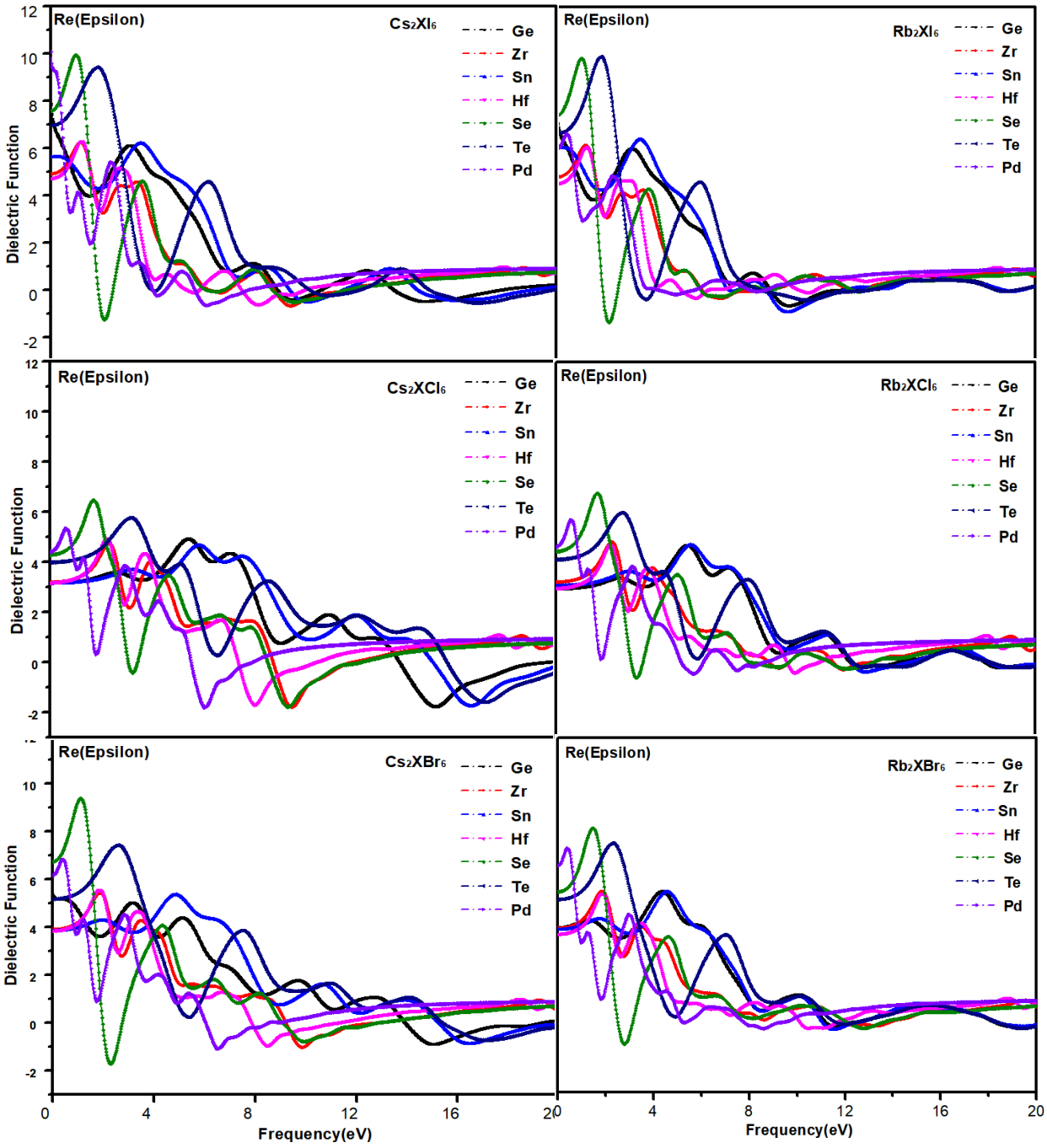

Fig. 8 Real part characteristic curve of dielectric

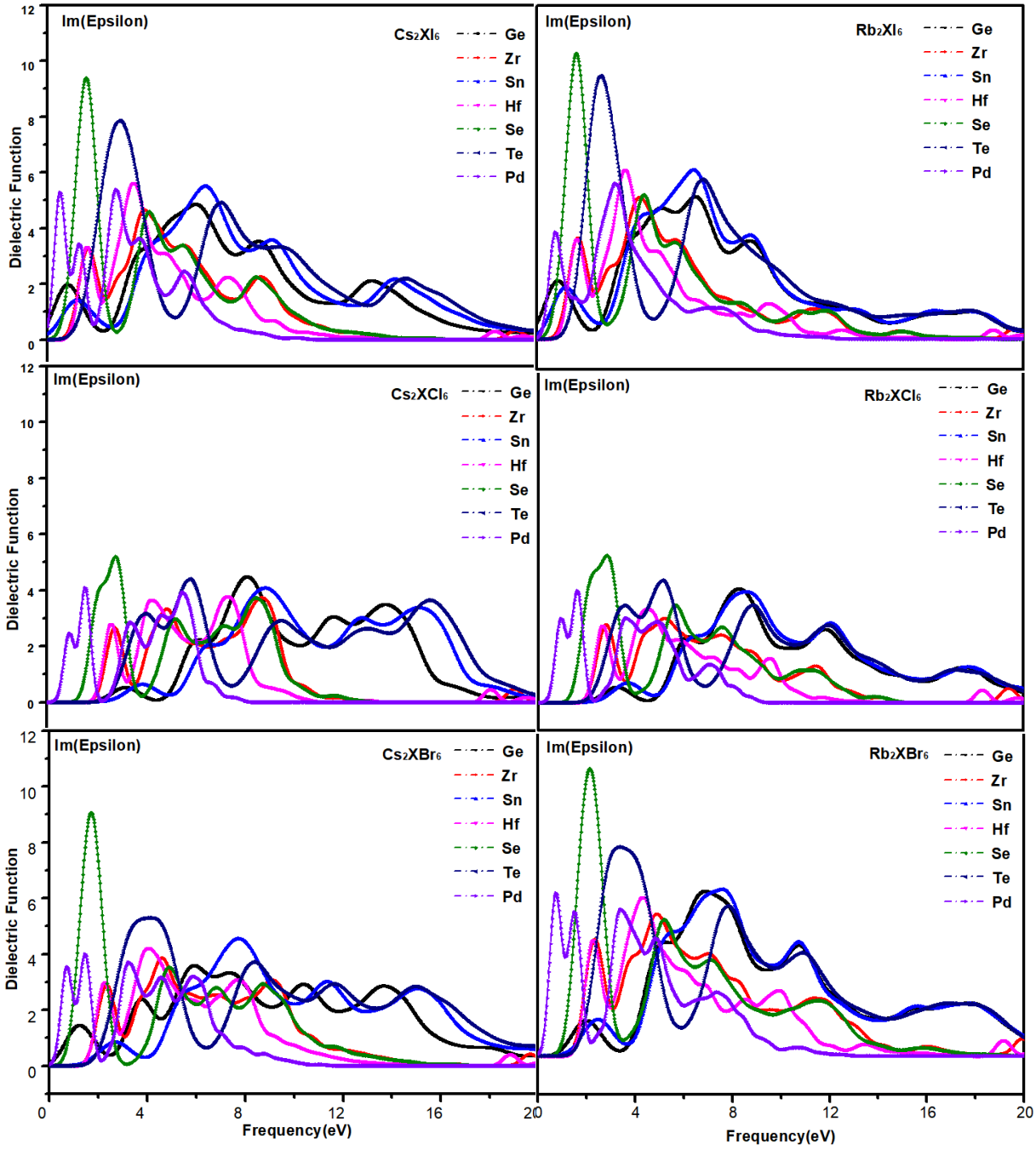

Fig. 9 Imaginary part characteristic curve of dielectric

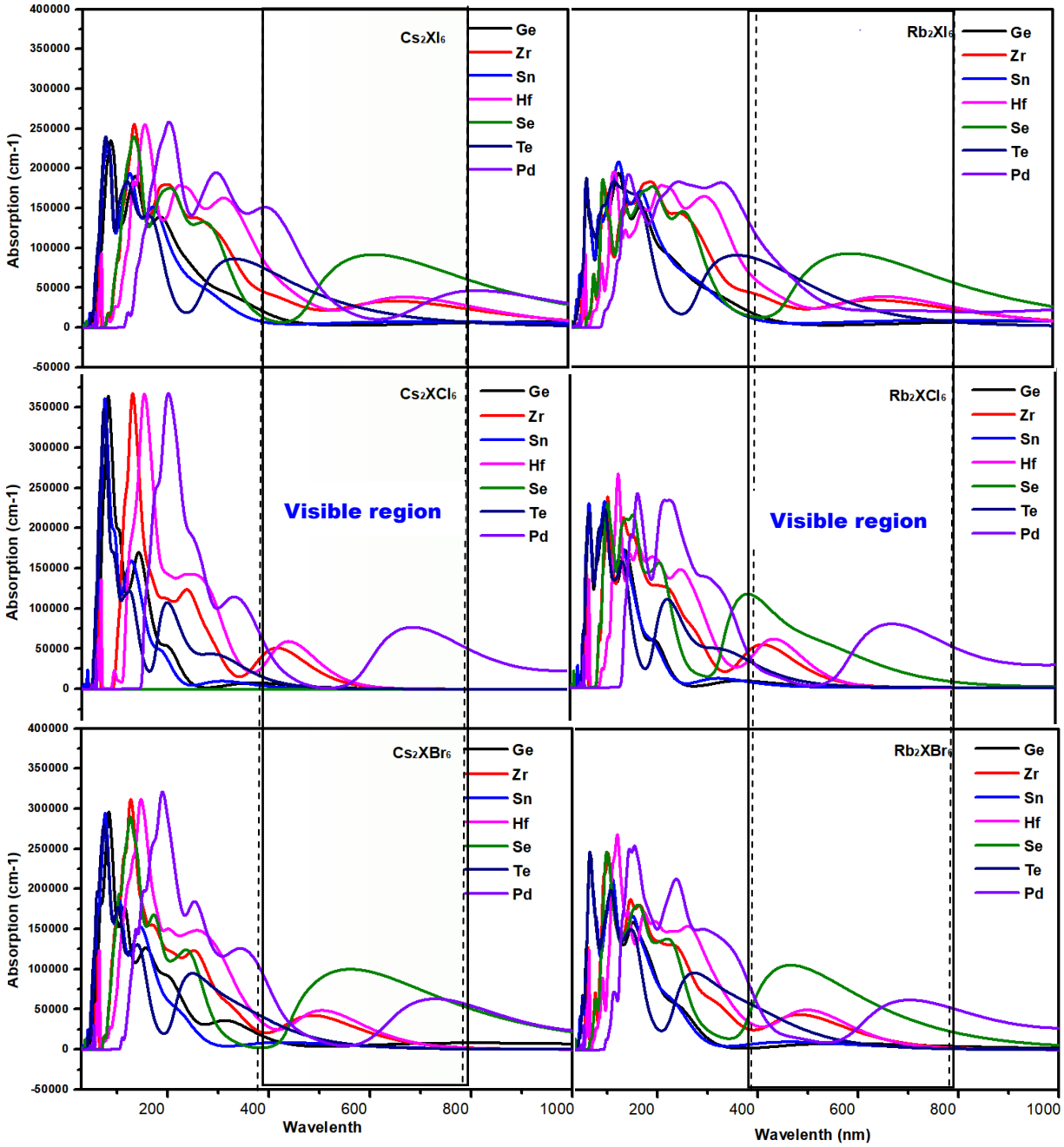

Fig. 10 Absorption spectra of 42 crystalline materials

than A_2XCl_6 and A_2XBr_6. The light absorption curves of seven tetravalent ions (Ge, Zr, Sn, Hf, Se, Te, Pd) compounds can be seen, their light absorption peaks are concentrated in the ultraviolet region, and those with better absorption effect in the visible light region have Se and Pd-containing materials. In contrast, the light absorption behavior of Rb_2XCl_6 in the visible region is poor, but the light absorption in the ultraviolet region is also considerable. Others with better

light absorption are halide perovskite materials containing Hf and Zr. From the absorption spectrum, it can be seen that Cs_2SeI_6, Rb_2SeI_6, Cs_2SeBr_6, Rb_2SeBr_6, Rb_2PdBr_6,Cs_2PdBr_6 are potential candidates for the absorption layer of solar cells.

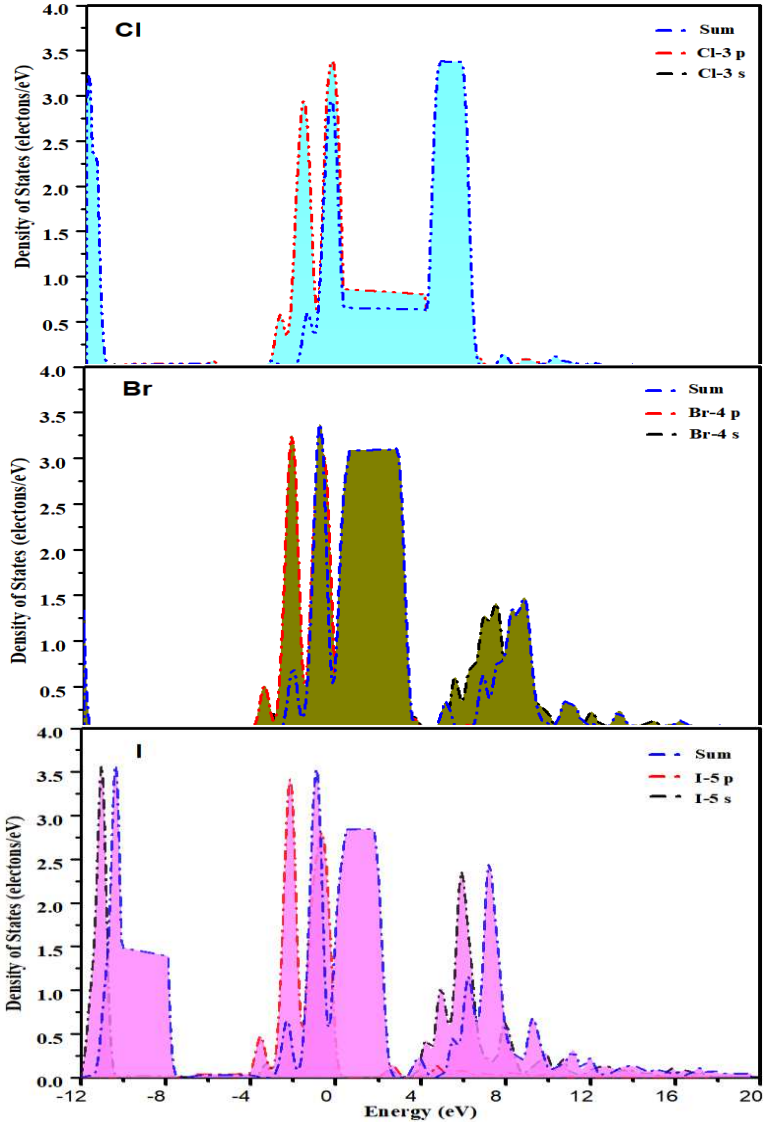

Fig. 11 Halogen element PDOS curve

Among halogen elements, as the atomic number increases, the ability of atoms to attract the outermost electrons gradually decreases, so the ability to obtain electrons decreases with the increase of atomic number. It can be seen from the PDOS curve in Fig. 11 that the curve peaks of Cl, Br, and I proceed in the direction of decreasing energy, and the energy of some electrons concentrated in the energy band decreases continuously.

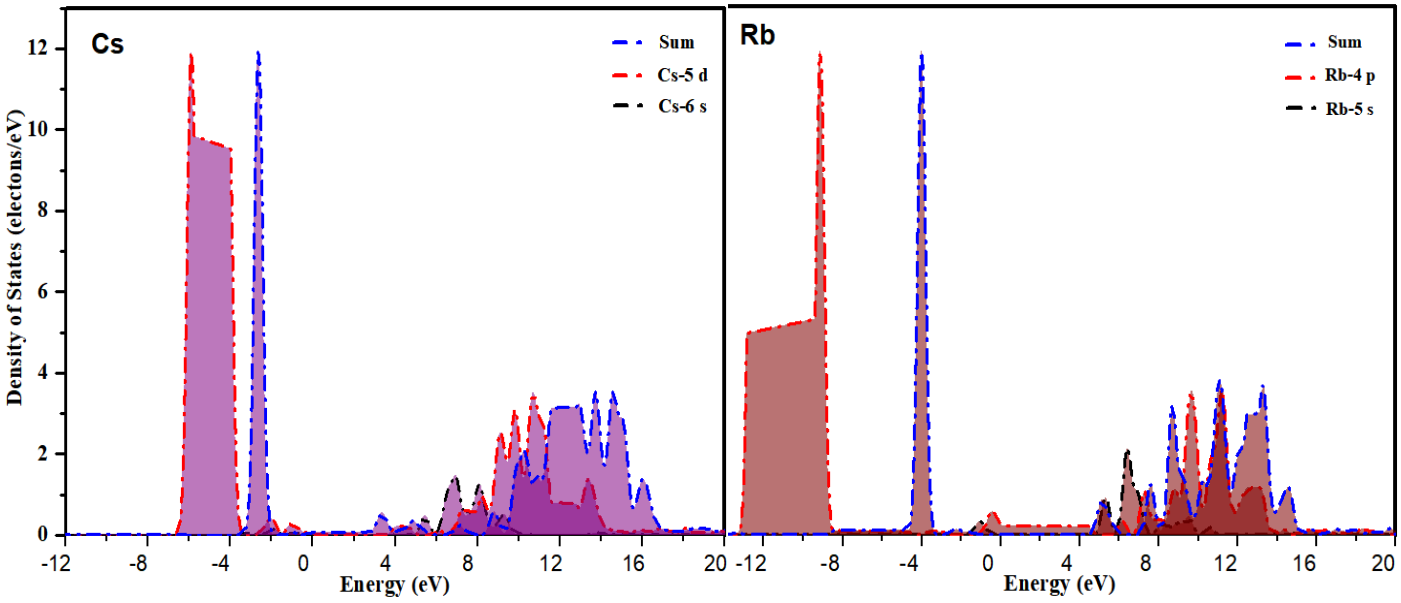

Fig. 12 PDOS curves of Cs and Pd

The PDOS curves of Cs and Rb are re-analyzed as shown in Figure 12. The contribution to Rb mainly comes from s and p electrons, and Cs mainly comes from s electrons and d electrons. Cesium (Cs) element, which is located in the sixth period, group IA. Its element is an active metal with a low melting point. It is easily oxidized in the air, and can react violently with water to generate hydrogen and explode. Cesium has no elemental form in nature, and is only rarely distributed in land and ocean in the form of salt. Cesium is an important material for the manufacture of vacuum devices and photocells. Rubidium is a kind of silver-white light metal, abbreviated as Rb. It is soft and waxy, and its chemical properties are more active than potassium. It is easy to release electrons under the action of light. This element easily reacts with oxygen to form complex oxides. Rubidium is widely used in energy, electronics, special glass, medicine and other fields. The reducibility of Rb is weaker than that of Cs, and the oxidative activity is stronger than that of Cs.

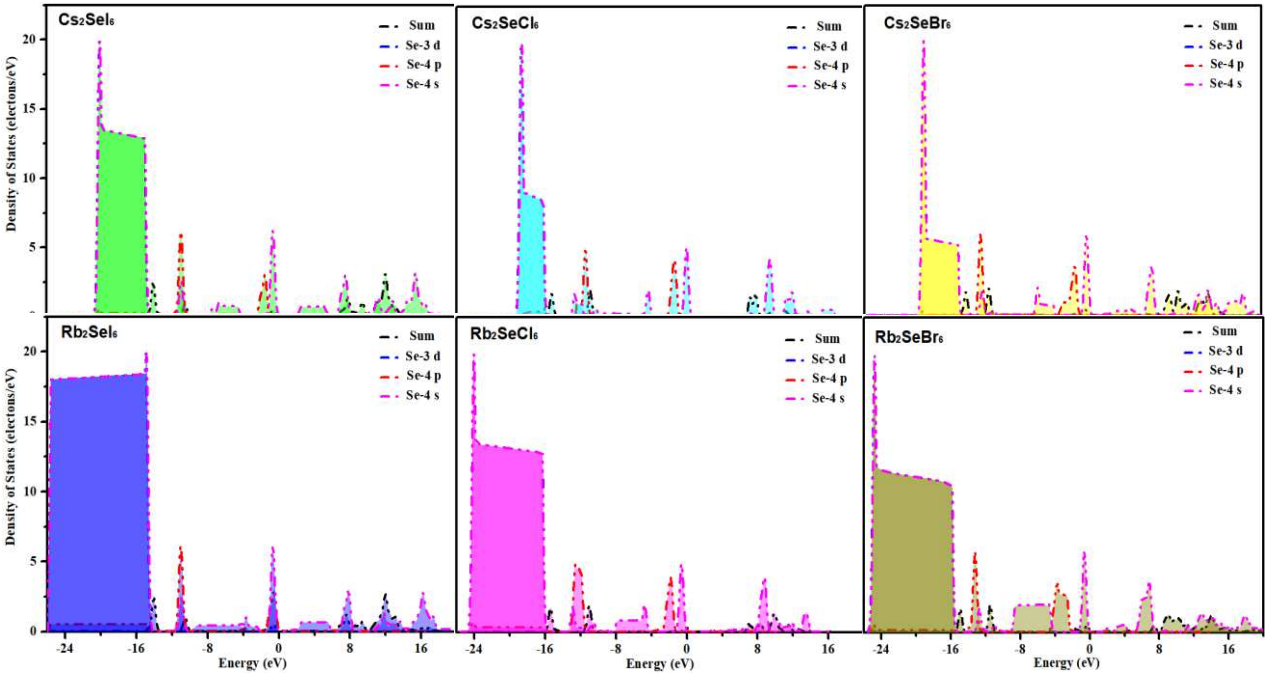

Fig. 13 PDOS curves of Se-containing perovskite materials

Since selenium(Cs)-containing perovskite compounds have good light absorption properties and band gap structures, this paper uses selenium-containing compounds as an example to calculate the PDOS curves of six crystals, involving electrons $3d^{10}$ $4s^2$ $4p^6$, and analyze the halogen elements in different combinations. The ability to gain and lose electrons. It can be seen from the PDOS curve of Fig. 13 that the atomic radius of Cl, Br, and I increases, and the extra-nuclear electrons increase accordingly, the binding ability of the nucleus to electrons decreases, the ability to obtain electrons decreases, and the oxidizing property decreases, so the horizontal comparison, the area covered by the density of states curve of Se widens.

The physical and chemical properties of the six tetravalent elements are as follows: Selenium symbol is abbreviated as Se, which is located in the fourth period VI A group (the 34th element) in the periodic table of chemical elements. It can be used as photosensitive material, electrolytic manganese industry catalyst, and the first ionization energy is 9.752 electron volts； Palladium is a platinum group element of the fifth periodic group VIII, abbreviated as Pd. It is a transition metal with good ductility and plasticity, and can be forged, rolled and drawn. It is chemically inactive and stable in air and humid environments at room temperature. Palladium is resistant to hydrofluoric, phosphoric, perchloric, hydrochloric, and sulfuric acid vapors； Hafnium is a metal element with symbol Hf, atomic number 72, and atomic weight 178.49. Its elemental substance is a lustrous silver-gray transition metal. Melting point 2227 ℃. Hafnium does not interact with

dilute hydrochloric acid, dilute sulfuric acid and strong alkali solution, and is often associated with zirconium in nature; Zirconium is a chemical element, the element symbol Zr atomic number is 40, the element is a high melting point metal. The surface of zirconium is easy to form an oxide film with luster. Corrosion resistant, zirconium readily absorbs hydrogen, nitrogen and oxygen. The surface of zirconium is easy to form an oxide film, which has luster and corrosion resistance.

4.2 Thermodynamical stability

To explore the thermodynamic stability of these crystals, we calculated their formation energies. For pure perovskites, the formation energy can be calculated using the following expression [49]：

$$\Delta E_1 = E(A_2BX_6) - 2E(AX) - E(BX_4) \tag{4}$$

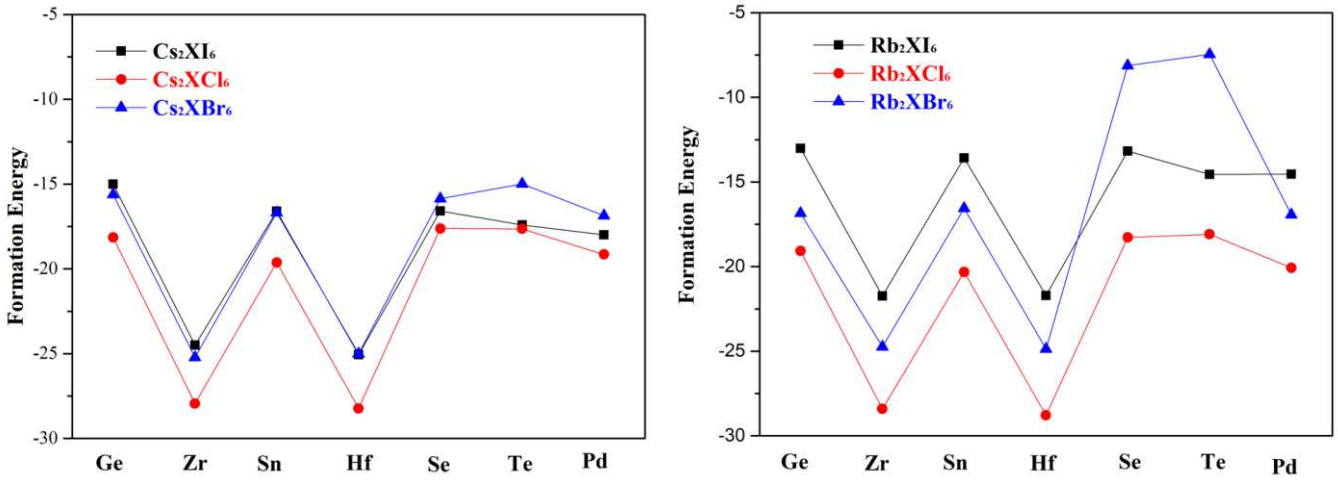

Fig. 14 The curve trend figure of formation energy

In general, the initial state of compound formation is the elemental state of A and B. It is necessary to first break the bond between the atoms of A and B, which requires absorbing energy, then forming AB, releasing energy, and the difference between the energy released and absorbed , is the heat of formation, which is equivalent to the heat of reaction of a chemical reaction. The more negative the formation energy, the more stable the compound. The calculation results are shown in Figure 14. The formation of compounds containing Cs and Rb elements is roughly the same, and the perovskite crystals containing Cs are more stable. Among these +4 valent elements, there are also Zr and Hf perovskite. The crystal structure is more stable. If the band gap size and

light absorption properties of Cs_2SeI_6, Rb_2SeI_6, Cs_2SeBr_6 and Rb_2SeBr_6 are considered comprehensively, they can be considered as ideal candidates for light absorption materials. In addition, Cs_2ZrI_6, Cs_2HfI_6, Rb_2ZrI_6, Rb_2HfI_6, Rb_2HfBr_6 are also superior in stability and band gap structure. Their light absorption behavior in the visible region is poor, but their light absorption in the ultraviolet region is also considerable.

4.3 Mechanical properties

Then, the mechanical stability of these materials is predicted from the calculated elastic moduli, which are calculated using finite strain theory [50]. The cubic crystal has three independent elastic constants (C_{11}、C_{12} and C_{44})。The natural mechanical stability criterion is given by: C_{11}- C_{12} > 0, C_{11} + 2C_{12} > 0, C_{44}> 0。 The calculated elastic constants of the 42 inorganic double perovskites are shown in Tables I to III. According to the above criteria, these compounds are mechanically stable. To differentiate between ductile and brittle materials, Pugh's ratio (B/G) and Poisson's ratio (v) are used. Poisson's ratio can be evaluated using the following formula：

$$\nu = (3B - 2G) / (6B + 2G) \quad (5)$$

where B and G are the bulk modulus and shear modulus, respectively. The critical B/G and values are 1.75 and 0.26 respectively [38, 44]. In other words, the composite is considered to be a ductile material when the B/G value is greater than 1.75 or the υ value is greater than 0.26, otherwise it is considered a brittle material. The calculation results are shown in Tables II-IV. The calculated value of elastic constants Cij, bulk modulus B (GPa), shear modulus G (GPa), Young's modulus E (GPa), Pugh's ratio K/G, and Poisson ratio (v) of cubic perovskite , Averaged sound velocity V(m/s)

Table II Elastic Modulus of Iodide Inorganic Perovskites

	C_{11}	C_{12}	C_{44}	B	E	G	v	V
Cs2GeI6	10.60+/- 0.11	1.45+/- 0.09	6.17+/- 0.001	4.48+/- 0.037	11.77	5.54	0.062	1250.65
Cs2HfI6	14.86+/- 0.39	3.17+/- 0.89	7.71+/- 0.005	7.06+/- 0.342	15.73	6.96	0.128	1336.07
Cs2PdI6	11.73+/- 1.15	4.21 +/- 1.63	6.19+/- 0.21	6.00+/- 0.56	11.7	4.94	0.19	1109.36
Cs2SnI6	11.64+/- 1.67	2.08+/- 0.24	8.32+/-0.001	5.27+/- 0.31	14.41	6.90	0.043	1338.68
Cs2TeI6	12.93+/-1.54	2.81+/- 1.29	6.85+/- 0.002	6.18+/- 0.55	13.83	6.18	0.13	1289.24
Cs2ZrI6	12.86+/- 0.21	2.27+/- 0.76	6.90+/- 0.016	5.84+/-0.29	13.92	6.30	0.10	1330.93
Cs2SeI6	11.49+/- 0.27	0.64+/- 0.19	5.97+/- 0.001	4.29+/- 0.10	11.91	5.74	0.037	1275.55
Rb2GeI6	9.25+/- 0.188	0.88+/- 0.10	5.32+/- 0.003	3.62+/- 0.05	10.01	3.63	0.04	1219.06
Rb2HfI6	11.07+/- 0.44	0.59+/- 0.89	6.35+/- 0.006	4.028+/-0.399	11.72	5.76	0.018	1265.34
Rb2PdI6	8.32+/- 0.435	4.25+/- 0.88	2.56+/- 0.129	6.33+/- 0.421	10.69	4.25	0.26	979.59

Rb2SeI6	10.38+/- 0.185	0.75+/- 0.177	4.99+/- 0.001	3.94+/- 0.080	10.43	4.92	0.059	1238.07
Rb2SnI6	12.72+/- 0.634	3.03+/- 1.10	8.64+/- 0.003	6.21+/- 0.435	15.39	7.07	0.088	1377.09
Rb2TeI6	11.23+/- 4.063	1.69+/- 2.92	1.15+/- 1.23	7.92+/- 2.19	3.36	1.19	0.407	0
Rb2ZrI6	9.95+/- 1.86	1.08+/- 0.184	6.02+/- 0.004	4.316+/-0.322	11.77	5.59	0.05	1303.08

Table III Elastic Modulus of Chloride Inorganic Perovskites

	C_{11}	C_{12}	C_{44}	B	E	G	ν	V
Cs2GeCl6	16.63+/- 0.908	3.77+/- 2.916	6.48+/- 1.02	8.16+/- 1.052	15.34	6.45	0.188	1589.73
Cs2HfCl6	15.71+/- 3.088	6.09+/- 2.444	10.99+/-0.025	7.95+/- 0.968	19.48	8.91	0.094	1672.25
Cs2PdCl6	14.88+/- 0.852	0.91+/- 0.979	6.34+/- 0.824	5.69+/-0.462	14.24	6.46	0.102	1511.75
Cs2SnCl6	15.21+/- 1.820	6.73+/- 0.655	10.99+/-0.001	9.18+/- 0.452	19.71	8.63	0.142	1697.10
Cs2TeCl6	17.09+/- 1.723	3.28+/- 0.601	8.20+/- 0.002	8.11+/- 0.284	18.07	8.00	0.022	1744.96
Cs2ZrCl6	13.6+/- 0.501	4.47+/- 0.927	10.04+/-0.002	7.33+/- 0.333	17.18	7.74	0.936	1659.38
Cs2SeCl6	13.30+/- 0.694	5.46+/- 0.274	5.98+/- 0.180	8.57+/- 0.516	13.11	5.22	0.255	1439.12
Rb2GeCl6	10.77+/- 0.144	3.93+/- 0.060	5.17+/- 0.112	5.98+/- 0.292	10.88	4.53	0.273	1442.78
Rb2HfCl6	13.48+/- 1.281	1.82+/- 0.959	9.16+/- 0.033	4.34+/- 0.794	14.07	6.79	0.584	1581.54
Rb2PdCl6	17.9+/- 2.626	6.31+/- 0.761	9.05+/- 0.833	9.95+/- 0.592	19.28	8.19	0.174	1774.54
Rb2SeCl6	14.86+/- 2.331	5.08+/- 0.340	6.70+/- 0.914	8.86+/- 0.581	15.56	6.42	0.212	1658.49
Rb2SnCl6	17.59+/- 2.979	7.71+/- 1.702	10.83+/-0.057	11.59+/-0.755	20.42	8.46	0.207	1774.97
Rb2TeCl6	16.78+/- 1.467	6.93+/- 1.054	8.53+/- 0.258	10.13+/-0.523	18.76	7.84	0.196	1789.21
Rb2ZrCl6	18.72+/- 1.255	6.51+/- 2.577	11.05+/- 0.001	9.13+/- 1.043	9.129	7.97	0.172	1747.20

Table IV Elastic moduli of bromide inorganic perovskites

	C_{11}	C_{12}	C_{44}	B	E	G	ν	V
Cs2GeBr6	11.17+/- 2.401	4.26+/- 0.518	8.923+/-0.006	6.41+/- 0.383	14.89	6.68	0.114	1342.40
Cs2HfBr6	15.89+/- 0.435	4.63+/- 1.470	11.63+/- 0.003	7.41+/- 0.569	19.74	9.21	0.072	1496.64
Cs2PdBr6	22.70+/- 6.342	-0.16+/- 1.109	5.61+/- 0.543	7.48+/- 1.074	18.02	8.19	0.519	1463.65
Cs2SnBr6	17.36+/- 0.393	3.01+/- 0.495	8.90+/- 0.006	8.01+/- 0.186	18.40	8.23	0.118	1555.68
Cs2TeBr6	13.02+/- 0.186	2.39+/- 0.128	8.53+/- 0.001	6.09+/- 0.067	15.75	7.36	0.069	1446.08
Cs2ZrBr6	15.18+/- 0.744	2.54+/- 1.790	9.09+/- 0.029	6.85+/- 0.706	17.08	7.78	0.098	1505.36
Cs2SeBr6	14.28+/- 0.741	2.03+/- 1.049	7.81+/- 0.001	5.98+/- 0.492	14.75	6.76	0.278	1424.76
Rb2GeBr6	10.81+/- 1.915	4.08+/- 0.823	9.29+/- 0.002	6.324+/-0.433	15.23	6.93	0.099	1402.02
Rb2HfBr6	15.11+/- 3.474	2.61+/- 1.006	8.49+/- 0.018	6.52+/-0.718	16.25	7.48	0.158	1481.47
Rb2PdBr6	13.54+/- 0.748	6.75+/- 0.923	8.13+/- 0.687	8.50+/- 0.492	15.61	6.49	0.201	1325.17
Rb2SeBr6	9.79+/- 0.535	2.27+/- 0.878	7.28+/- 0.002	5.06+/-0.408	11.23	4.90	0.146	1195.87
Rb2SnBr6	18.77+/- 0.152	5.23+/- 0.673	9.19+/- 0.010	9.79+/- 0.266	19.29	8.23	0.111	1600.55
Rb2TeBr6	11.95+/- 2.248	4.02+/- 0.322	2.83+/- 0.536	7.58+/- 0.359	8.44	3.19	0.363	1014.96
Rb2ZrBr6	13.68+/- 2.566	5.48+/- 0.863	9.27+/- 0.003	8.69+/- 0.599	17.85	7.69	0.464	1541.25

In order to analyze the stability of the crystal in more detail, we plotted three elastic constants C_{11}, C_{12} and C_{44} sufficient to explain the complete mechanical

behavior of cubic symmetry as shown in Figure 15. It is easy to conclude that they meet the criteria of C_{11}-C_{12}>0, C_{44}>0, and C_{11}+2C_{12}>0, indicating that their mechanical stability is relatively good.

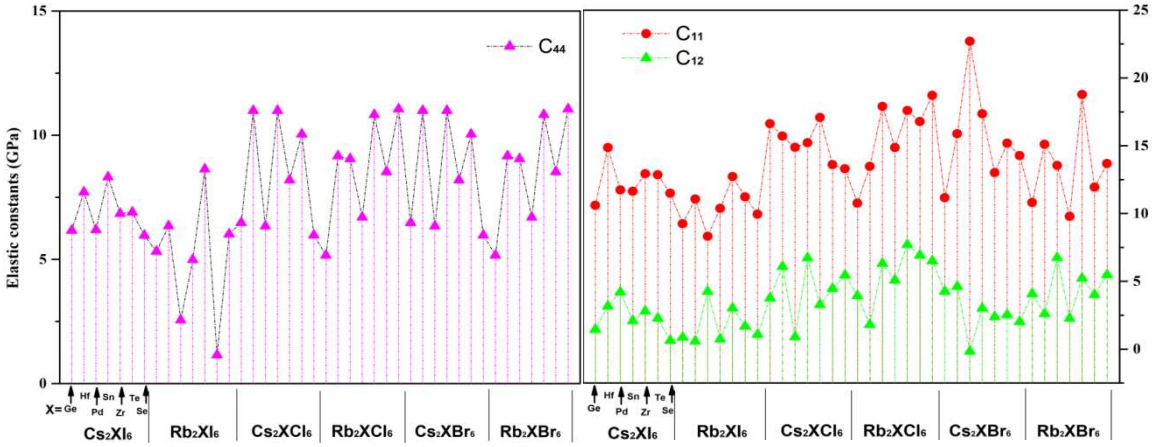

Fig. 15 Intuitive graph of elastic modulus C_{11}, C_{12}, C_{44}

The critical limit of 1.75 for the Pugh ratio (B/G) distinguishes the brittle (B/G <1.75) and ductile (B/G >1.75) behavior of the studied material. The values reported in Tables I~III show the ductility behavior, the Poisson's ratio (υ) further ensures ductility, and the critical limit for ductile materials is υ >0.26 [50,51]。Figure 16 is a graph showing its Poisson's ratio and Puhg ratio, and the comparison shows that Rb_2TeI_6, Cs_2TeI_6, Rb_2HfCl_6, Cs_2PdBr_6, Cs_2SeBr_6, Rb_2TeBr_6, Rb_2SeBr_6 are more ductile, while others are more brittle.

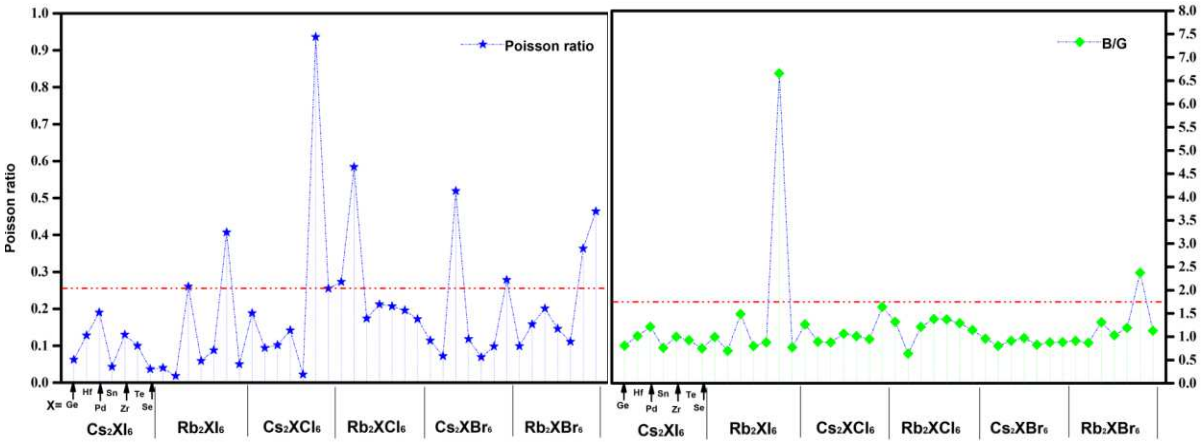

Fig. 16 Intuitive plot of Poisson's ratio and B/G

5. Conclusion

Here we report the photoelectric conversion properties and stability of 42 inorganic double perovskite materials based on density functional theory. Starting from the construction of double perovskite crystal structures, the data mining algorithm in informatics is introduced into high-throughput computing data analysis. The study found the valence band maximum (VBM) and conduction band minimum (CBM) of 42 compounds, and we compared the band gaps of two efficient organic/inorganic perovskite materials. Among them, the tolerance factors of 39 kinds of crystals are between 0.8 and 1.10. Then, the important parameters such as dielectric function, PDOS curve, elastic modulus, shear modulus and Poisson's ratio of the crystals are analyzed. And the maximum value of the valence band of these materials and the size of the valence band of the electron transport layer material, hole transport layer and back electrode material are analyzed, which is helpful to analyze the efficiency of carrier migration of these materials. Among the above 14 materials with band gaps between 1.33 and 2.40, (Cs_2ZrI_6, Cs_2HfI_6, Cs_2SeI_6, Cs_2TeI_6, Rb_2HfI_6, Rb_2SeI_6, Rb_2TeI_6, Rb_2GeCl_6, Rb_2HfBr_6) the minimum edge of the conduction band of these materials is greater than -4.6eV, and the maximum value of the valence band Below 5.4 eV, the band gap of Rb_2SnBr_6 and Rn_2SnI_6 are large, which may be used in the ultraviolet region. From the absorption spectrum, the light absorption curves of Cs_2SeI_6, Cs_2SeBr_6 Rb_2SeI_6, Rb_2SeBr_6 and Rb_2SeCl_6 fall in a relatively large range in the visible light region. Further considering the stability factor, the formation energy is an important factor for the thermodynamic stability of the reaction. The results show that the formation of compounds containing Cs and Rb elements is roughly the same, and the perovskite crystals containing Cs are more stable, with several +4 valences. Among the elements, the perovskite crystal structure containing Zr and Hf is more stable. Among the several +4 valent elements, the perovskite crystal structure containing Zr and Hf is more stable. Combined with its band gap size and light absorption properties, Cs_2SeI_6, Rb_2SeI_6, Cs_2SeBr_6 and Rb_2SeBr_6 can be used as ideal candidates for light absorption materials. This work can not only guide experiments and design experiments rationally, but also reduce research and development costs, shorten research time, and improve the success rate of material design. Above all, it provides an important theoretical basis for the industrialization of perovskite solar cells.

Availability of Data and Materials

The datasets used and analysed during the current study available from the corresponding

author on reasonable request.

Acknowledgment

This work is supported by Key scientific research Program of Higher Education of He’nan Province [No. 22B140005] and [No.22A460026].

References

[1] Zhou, L., Xu, Y. F. , Chen, B. X., Kuang, D. B., Su, C.Y., Synthesis and photocatalytic application of stable lead-free $Cs_2AgBiBr_6$ perovskite nanocrystals, Small, **14**, 1703762.(2018).

[2] Reshak, A. H., , Ab initio study of TaON, an active photocatalyst under visible light irradiation. Phys. Chem. Chem. Phys. **16**, 10558. (2014).

[3] Kim, H. S., Lee, C. R., Im, J. H., Lee, K. B., Moehl, T., Marchioro, A., Moon, S. J., Humphry-Baker, R., Yum, J.-H., Moser, J.E., Gratzel, M. and Park, N.-G., Lead Iodide Perovskite Sensitized All-Solid-State Submicron Thin Film Mesoscopic Solar Cell with Efficiency Exceeding 9%. Scientific Reports, **2**, 591. (2012).

[4] Tang, y., Jihua Zhang, J. H., Zhong, X. L., Wang, Q. J., Zhang, H., Ren, C. L., Wang, J. B., Revealing the structural, electronic and optical properties of lead-free perovskite derivatives of Rb2SnX6(X = Cl, Br and I): A theory calculation，Solar Energy, **190**, 272–277, (2019).

[5] Xiao, Z., Lei, H., Zhang, X., Zhou, Y., Hosono, H., and Kamiya, T., Ligand-hole in [SnI6] unit and origin of band gap in photovoltaic perovskite variant Cs_2SnI_6. Bull. Chem. Soc. Jpn. **88**, 1250–1255.(2015).

[6] Qiu, X., Cao, B., Yuan, S., Chen, X., Qiu, Z., Jiang, Y., et al., From unstable $CsSnI_3$ to air-stable Cs_2SnI_6: A lead-free perovskite solar cell light absorber with bandgap of 1.48eV and high absorption coefficient. Solar Energy Mater. Solar Cells, **159**, 227–234. (2017).

[7] Guechi N., Bouhemadou A., Omran S.B., Bourzami A., Louail L., Elastic, Optoelectronic and Thermoelectric Properties of the Lead-Free Halide Semiconductors Cs2AgBiX 6 (X = Cl, Br): Ab Initio Investigation, J. Electron. Mater. **4**, 1533–1545. (2017).

[8] T. Ishibe, A. Tomeda, K. Watanabe, Y. Kamakura, N. Mori, N. Naruse, Y. Mera, Y. Yamashita, Y. Nakamura, Methodology of Thermoelectric Power Factor Enhancement by Controlling Nanowire Interface, ACS Appl. Mater. Interfaces, **10**, 37709–37716. (2018)

[9] Sa, R. J., Wei, Y. C., Zha, W. Y., Liu, D. W., A first-principle study of the structural, mechanical, electronic and optical properties of vacancy-ordered double perovskite Cs_2TeX_6 (X =

Cl, Br, I), Chemical Physics Letters, **754** , 137538, (2020).

[10] Zhang Y., Tso C.Y., Iñigo J.S., Liu S., Miyazaki H., Chao C, Y. H., Yu K.M., Perovskite thermochromic smart window : Advanced optical properties and low transition temperature, Appl. Energy **254**, 113690. (2019).

[11] Peedikakkandy, L., Naduvath, J., Mallick, S., Bhargava, P., Lead free, air stable perovskite derivative Cs2SnI6 as HTM in DSSCs employing TiO_2 nanotubes as photoanode, Materials Research Bulletin, **108**, 113–119. (2018).

[12] Haque, E., Hossain, M. A., Origin of ultra-low lattice thermal conductivity in Cs_2 $BiAgX_6$ (X = Cl, Br) and its impact on thermoelectric performance, J. Alloys Compd. 748 , 63–72. (2018).

[13] Jeong M Y, Choi I W, Yim K H, Jeong S J, Kim M J, Choi S J, Cho Y J, An J H, Kim H B, Jo Y , Kang S H, Bae J H, Lee C W, Kim D S and Yang C, Large-area perovskite solar cells employing spiro-Naph hole transport material. Nature Photon. 16, 119–125，(2022).

[14] Yin, X., Song, Z., Li, Z. & Tang, W., Toward ideal hole transport materials: a review on recent progress in dopant-free hole transport materials for fabricating efficient and stable perovskite solar cells, Energy Environ. Sci., **13**, 4057–4086 . (2020).

[15] Jeong, M, Choi I W, Go E M， Cho Y， Kim M，Lee B, Jeong S，Jo Y， Choi H W, Lee J., Stable perovskite solar cells with efficiency exceeding 24.8% and 0.3-V voltage loss. Science, **369**, 1615–1620. (2020).

[16] Chen H, Chen Y T, Zhang T Y, Liu X M, Wang X T, Zhao Y X., Advances to High-Performance Black-Phase $FAPbI_3$ Perovskite for Efficient and Stable Photovoltaics, Small Struct., **2**, 2000130. (2021).

[17] Lin R X, Xu J, Wei M Y, Wang Y R, Qin Z Y, Liu Z, Wu J L, Xiao K, Chen B, Park S M, Chen G, Atapattu H R, Graham K R, Xu J, Zhu J, Li L D, Zhang C F, Sargent E H and Tan H., All-perovskite tandem solar cells with improved grain surface passivation. Nature, **603**, 73–78 .(2022).

[18] Jiang X Y, Wang F, Wei Q, Li H S, Shang Y Q, Zhou W J,Wang C, Cheng P H, Chen Q, Chen L W and Ning Z J., Advances to High-Performance Black-Phase FAPbI3 Perovskite for Efficient and Stable Photovoltaics, Nature Communications., **11**:1245,1-7. (2020).

[19] Liu X, Wang Y B, Wu T H, He X, Meng X Y, Barbaud J L, Chen H, Segawa H, Yang X D and Han L Y., Templated growth of $FASnI_3$ crystals for efficient tin perovskite solar cells, Nature

Communications., **11**:2678,1-7. (2020).

[20] Aydin E, Allen T G, Bastiani M D, Xu L J, Ávila J, Salvador M, Kerschaver E V and Stefaan Wolf D., Interplay between temperature and bandgap energies on the outdoor performance of perovskite/silicon tandem solar cells, Nature Energy, **5**, 851–859. (2020).

[21] Li C W, Song Z N, Chen C, \ Xiao C X, Subedi B, Harvey S P, Shrestha N, Subedi K K, Chen L, Liu D C, Li Y, Kim Y W, Jiang C S, Heben M J, Zhao D W, Ellingson R J, Podraza N J, Mowafak A J and Yan Y F., Low-bandgap mixed tin–lead iodide perovskites with reduced methylammonium for simultaneous enhancement of solar cell efficiency and stability, Nature Energy, **5**, 768–776. (2020).

[22] Xiao K, Lin R X, Han Q L, Hou Y, Qin Z Y, Nguyen H T, Wen J, Wei M Y, Yeddu V, Saidaminov M, Gao Y, Luo X, Wang Y R, Gao H, Zhang C F, Xu J, Zhu J, Sargent E H and Tan H R., All-perovskite tandem solar cells with 24.2% certified efficiency and area over 1 cm2 using surface-anchoring zwitterionic antioxidant, Nature Energy, **5**, 870–880. (2020).

[23] Stranks, S. D.; Snaith, H. J., Metal-halide perovskites for photovoltaic and light-emitting devices. Nature nanotechnology, **10**, 391–402.(2015).

[24] O' Regan, B. and Grätzel, M., A low-cost, high-efficiency solar cell based on dye-sensitized colloidal TiO_2 films. Nature , **353** , 737–739 . (1991).

[25] Noh, J.H., Im, S.H., Heo, J.H., Mandal, T.N. and Seok, S.I., Chemical Management for Colorful, Efficient, and Stable Inorganic-Organic Hybrid Nanostructured Solar Cells. Nano Letters, **13**, 1764-1769. (2013).

[26] Leijtens, T., Eperon, G. E., Pathak, S., Abate, A., Lee, M. M., Snaith, H. J., Overcoming ultraviolet light instability of sensitized TiO_2 with meso-superstructured organometal trihalide perovskite solar cells. Nat. Commun. **4**, 2885. (2013).

[27] Green, M.A., Baillie, A.H., Snaith, H.J., The emergence of perovskite solar cells, Nat. Photon. **8**, 506–514.(2014).

[28] Giles E Eperon, Tomas Leijtens , Kevin A Bush, Rohit Prasanna, Thomas Green, Jacob Tse-Wei Wang, David P McMeekin, George Volonakis, Rebecca L Milot, Richard May, Axel Palmstrom, Daniel J Slotcavage, Rebecca A Belisle, Jay B Patel, Elizabeth S Parrott, Rebecca J Sutton, Wen Ma, Farhad Moghadam, Bert Conings, Aslihan Babayigit, Hans-Gerd Boyen , Stacey Bent, Feliciano Giustino, Laura M Herz, Michael B Johnston , Michael D McGehee , Henry J

Snaith, Perovskite-perovskite tandem photovoltaics with optimized band gaps, Science **354**, 861–865. (2016).

[29] Cruz, S.H.T., Hagfeldt, A., Saliba, M., Methylammonium-free, high-performance, and stable perovskite solar cells on a planar architecture, Science **362**, 449–453. (2018).

[30] Volonakis, G., Filip, M.R., Haghighirad, A.A., Sakai, N., Wenger, B., Snaith, H. J., Giustino, F., Lead-Free Halide Double Perovskites via Heterovalent Substitution of Noble Metals, J. Phys. Chem. Lett. **7**, 1254–1259. (2016).

[31] Slavney, A.H., Hu, T., Lindenberg, A.M., Karunadasa, H.I., , A Bismuth-Halide Double Perovskite with Long Carrier Recombination Lifetime for Photovoltaic Applications, J. Am. Chem. Soc. **138**, 2138–2141. (2016).

[32] Roknuzzaman M. and Akther Hossain, A. K. M., Effect of metal doping on the visible light absorption, electronic structure and mechanical properties of non-toxic metal halide CsGeCl3, Org. Electron. **59**, 99–106. (2018).

[33] Peedikakkandy, L. and Bhargava, P., , Composition dependent optical, structural and photoluminescence characteristics of cesium tin halide perovskites, RSC Adv., ,6, 19857-19860. (2016).

[34] Hohenberg, P. and Kohn, W., , Inhomogeneous Electron Gas, Phys. Rev. **136**, B864. (1964).

[35] Kohn, W. and Sham, L. J., , Self-Consistent Equations Including Exchange and Correlation Effects, Phys. Rev. **140,** A1133. (1965).

[36] Segall, M. D., Lindan, P. L. D., Probert, M. J., Pickard, C. J., Hasnip, P. J., Clark, S. J. and Payne, M. C., , First-principles simulation: ideas, illustrations and the CASTEP code, J. Phys.: Condens. Matter **14** , 2717–2744, (2002).

[37] Kresse, G., Furthmüller, J.,. Efficient iterative schemes for ab initio total-energy calculations using a plane-wave basis set. Phys. Rev. B. **54**, 11169–11186. (1996).

[38] Perdew, J. P., Burke, K. and Ernzerhof, M., Efficient iterative schemes for ab initio total-energy calculations using a plane-wave basis set, Phys. Rev. Lett., **77**, 3865-3868. (1996).

[39] Finazzi, E., Di Valentin, C., Pacchioni, G. and Selloni, A., Excess electron states in reduced bulk anatase TiO2: Comparison of standard GGA, GGA+U, and hybrid DFT calculations, J. Chem. Phys., **129**, 154113. (2008).

[40] Belsky, A.; Hellenbrandt, M.; Karen, V. L.; Luksch, P., New Developments in the Inorganic Crystal Structure Database (ICSD): Accessibility in Support of Materials Research and Design. Acta Crystall ographica Section B:,**58**, 364−369. (2002).

[41] Bergerhoff, G.; Hundt, R.; Sievers, R.; Brown, I. D., The Inorganic Crystal Structure Data Base. J. Chem. Inf. Model. **23**, 66−69. (1983).

[42] Maughan, A. E., Ganose, A. M., Candia, A. M., Granger, J. T., Scanlon, D. O., Neilson, J. R., Anharmonicity and Octahedral Tilting in Hybrid Vacancy-Ordered Double Perovskites, Chem. Mater., **30**, 472, (2017).

[43] Malak Azmat Ali, Thamraa Alshahrani, G. Murtaza, Defective perovskites Cs_2SeCl_6 and Cs_2TeCl_6 as novel high temperature potential thermoelectric materials, Materials Science in Semiconductor Processing, **127**, 105728, 1-7. (2021).

[44] Tahani I. Al-Muhimeed, A. I. Aljameel, Abeer Mera, Saher Saad, Ghazanfar Nazir , Hind Albalawi, S. Bouzgarrou, H. H. Hegazy and Q. Mahmood, First principle study of optoelectronic andmechanical properties of lead-free double perovskites Cs_2SeX_6 (X = Cl, Br, I), Journal Of Taibah University for Science, **16**, 1, 155–162. (2022).

[45] Kang, B. Y. and Biswas, K., Carrier Self-Trapping and Luminescence in Intrinsically Activated Scintillator: Cesium Hafnium Chloride (Cs_2HfCl_6), The Journal of Physical Chemistry, **120**(22), 12187-12195. (2016).

[46] Liu, D. W., Sa, R. J., Theoretical study of Zr doping on the stability, mechanical, electronic and optical properties of Cs_2TiI_6, Optical Materials, **110**, 110497. (2020).

[47] Li, C., Lu, X., Ding, W., Feng, L., Gao, Y., Guo, Z., Formability of ABX_3 (X = F, Cl, Br, I) halide perovskites, Acta Cryst. B, **64**, 702-707, (2008).

[48] Saha, S., Sinha, T. P., Mookerjee, A., Electronic structure, chemical bonding, and optical properties of paraelectric $BaTiO_3$, Phys. Rev. B, **62**, 8828. (2000).

[49] Liu, D. W., Zha, W. Y., Yuan, R. S., Chen, J. M. and Sa, R. J., First-principles study on the optoelectronic properties of mixed-halide double perovskites Cs2TiI6-xBrx, New Journal of Chemistry, **44**, 13613-13618, (2020).

[50] Roknuzzaman, M., Ostrikov, K., Wang, H., Du, A. .and Tesfamichael, T., Towards lead-free perovskite photovoltaics and optoelectronics by ab-initio simulations. *Sci. Rep.*, **7**, 14025. (2017).

[51] Mahmood, Q., Ghrib, T., Rached, A., Laref, A., Kamran, M. A., Probing of mechanical,

optical and thermoelectric characteristics of double perovskites Cs2GeCl/Br6 by DFT method, Materials Science in Semiconductor Processing, **112**, 105009, (2020).